ACS Photonics

pubs.acs.org/journal/apchd5

Letter

Near-Field Imaging of Magnetic Complex Mode Volume

Niccolò Caselli,* Tong Wu, Guillermo Arregui, Nicoletta Granchi, Francesca Intonti, Philippe Lalanne, and Massimo Gurioli

Cite This: *ACS Photonics* 2021, 8, 1258–1263

Read Online

ACCESS | Metrics & More | Article Recommendations

ABSTRACT: The non-Hermitian nature of confined photonic modes is described by the electric complex modal volume, V_E, which represents a key parameter that leads to counterintuitive effects, such as negative modal contribution to the local density of states and non-Lorentzian lineshapes. Here, we address the magnetic counterpart of V_E by means of near-field perturbation experiments in a photonic crystal slab cavity. We study the relevant role played by the imaginary part of the magnetic modal volume, V_H, which can increase the quality factor of the confined modes by means of a local external magnetic perturbation. We show how a mapping of the spatial distribution of both the real and imaginary parts of V_H can be inferred by near-field experiments employing Al-covered near-field tips. Our findings deepen the role of the magnetic component of light and could open a new route in employing metamaterials, magnetic quantum emitters, and topological photonics.

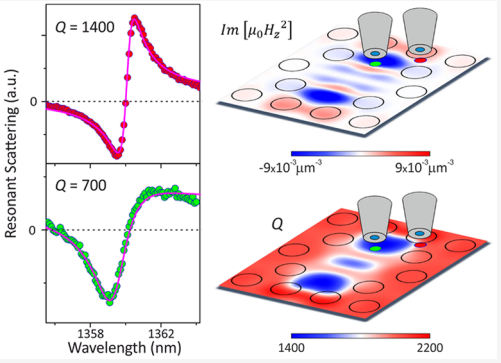

KEYWORDS: *electromagnetic resonance, magnetic light, photonic microcavity, cavity perturbation theory, mode volume*

Recently, important progresses have been achieved on the description of photonics as a non-Hermitian open system, and within quasinormal mode (QNM) theory, any optical resonator can be described by a set of n modes with normalized complex electric fields $\tilde{\mathbf{E}}_n(\mathbf{r})$ and complex frequencies $\tilde{\omega}_n = \omega_n - i\Gamma_n$, with ω_n the resonant frequency and Γ_n the coherence damping rate.[1−4] The phase of each mode is a well-defined quantity that can be measured, and ultimately, it leads to deep modifications of the common picture of the Purcell[5] effect and perturbation theory.[6−8] Most of these phenomena can be described by introducing the concept of complex modal volume. The complex-valued electric modal volume, for the nth QNM of a given optical resonator, probed by an electric dipole $\mathbf{p} = p\mathbf{u}$ and at the position $\mathbf{r}$ is defined as:[1]

$$\tilde{V}_n^E(\mathbf{r}) = [2\varepsilon_o\varepsilon(\mathbf{r})(\tilde{\mathbf{E}}_n(\mathbf{r})\cdot\mathbf{u})^2]^{-1} \quad (1)$$

where $\varepsilon(\mathbf{r})$ is the relative dielectric constant. When an electric dipolar perturber is placed in the vicinity of the cavity, the complex frequency change $\Delta\tilde{\omega}_n$ is proportional to $\frac{\Delta\tilde{\omega}_n}{\tilde{\omega}_n} = -\frac{\alpha}{2\tilde{V}_n^E(\mathbf{r})}$ with α being the polarizability of the perturber. The imaginary part of the electric modal volume is related to non-Hermitian effects, for example, the change of the Q factor of the mode by constructive or destructive interference between the scattered fields of the cavity and the scatterer. The powerfulness of $\mathrm{Im}(\tilde{V}_n^E)$ in predicting the Q change has recently been confirmed with near-field experiments, showing that the map of $\mathrm{Im}(\tilde{V}_n^E)$ fully explains the tip-induced change of Q and that the electric complex mode is directly observable and carries true physical significance.[7] On the other hand, the imaginary part of the electric modal volume imposes a non-Lorentzian local density of states and therefore modifies the Purcell effect in the spontaneous emission of a quantum emitter with an allowed dipole electric transition.[2] It has been evidenced by several experiments, even in systems with very high Q, that the imaginary part of the electric modal volume fully defines the asymmetry parameter of the Fano local density of states (LDOS) profile.[5] Recent results on hybrid systems reported a way to engineer arbitrary Fano lineshapes in the local density of optical states.[9]

The growing interest of magnetic light−matter interaction in metamaterials and topological photonics[10−12] advocates for the introduction of an equivalent mode volume for the magnetic fields $\tilde{\mathbf{H}}_n(\mathbf{r})$ of the nth resonant mode, probed by a magnetic dipole $\mathbf{m} = m\mathbf{u}$,

$$\tilde{V}_n^H(\mathbf{r}) = -[2\mu_0\mu(\mathbf{r})(\tilde{\mathbf{H}}_n\cdot\mathbf{u})^2]^{-1} = -[2\mu_0(\tilde{\mathbf{H}}_n\cdot\mathbf{u})^2]^{-1} \quad (2)$$

where the last expression holds for $\mu(\mathbf{r}) = 1$, that is, the usual photonic cavity made by dielectric (and nonmagnetic)

Received: December 23, 2020
Published: April 14, 2021

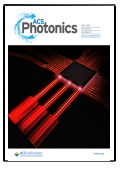

https://doi.org/10.1021/acsphotonics.0c01943
ACS Photonics 2021, 8, 1258–1263

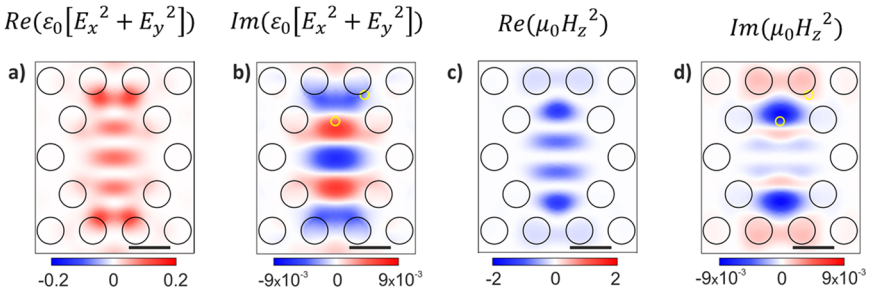

Figure 1. Computation of the spatial distributions of the real and imaginary parts of the relevant electric (a, b) and magnetic (c, d) inverse modal volume of a D2 cavity with holes of diameter 206 nm (black empty circles) and a lattice constant of 331 nm; the units are in μm^{-3}. The black scale bars in the figures are 300 nm. The maps are computed in air on a plane placed 20 nm above the membrane surface. The yellow circles in (b) and (d) highlight the regions where the SNOM data of Figure 2 are acquired.

materials. Note that the minus sign in the definition arises from the normalization condition of the QNM, which is a tricky aspect long debated.[1,13] Here we use the following:[2]

$$\iiint (\varepsilon_o \varepsilon(\mathbf{r})\tilde{\mathbf{E}}_n(\mathbf{r})^2 - \mu_0 \tilde{\mathbf{H}}_n(\mathbf{r})^2) \mathrm{d}^3 r = 1 \tag{3}$$

where the integral extends to the whole volume, including the perfect matching layer (PML) regions whenever FDTD simulations are used. In order to grasp the need of the minus in eq 2 as well as in the normalization integral in eq 3, let us remember that, for a high Q and spectrally isolated mode, the normalized electric field $\tilde{\mathbf{E}}_n(\mathbf{r})$ is almost real and the normalized magnetic field $\tilde{\mathbf{H}}_n(\mathbf{r})$ is almost imaginary.[1] Therefore, in eq 2 we add the minus sign to require that the real part of the magnetic volume is positive, as intuitively expected.

We stress that, in analogy to its electric counterpart, $\tilde{V}_n^H(\mathbf{r})$ defines the Purcell effect of an optical magnetic dipole transition via the nth mode of an optical resonator, by the following formula:

$$\gamma_n(\mathbf{r}, \omega) = \frac{2\mu_0}{\hbar} |\mathbf{m}|^2 \mathrm{Re}\left[\frac{Q_n}{\tilde{V}_n^H(\mathbf{r})}\right] \frac{\omega}{\omega_n} \frac{\Gamma_n^2}{(\omega - \omega_n)^2 + \Gamma_n^2} \times \left(1 + \frac{\mathrm{Im}[\tilde{V}_n^H(\mathbf{r})]}{\mathrm{Re}[\tilde{V}_n^H(\mathbf{r})]} \frac{\omega - \omega_n}{\Gamma_n}\right) \tag{4}$$

Here we consider a quantum emitter with magnetic dipole moment $\mathbf{m} = m\mathbf{u}$ embedded in a photonic cavity at position $\mathbf{r}$ and the quality factor of the mode is $Q_n = \omega_n/(2\Gamma_n)$.

The introduction of a magnetic mode volume also allows for the prediction of the complex frequency shift of the mode when the cavity is perturbed by a point-like object with both electric and magnetic responses:

$$\frac{\Delta\tilde{\omega}_n}{\tilde{\omega}_n} = -\frac{\alpha}{2\tilde{V}_n^E(\mathbf{r})} - \frac{\beta}{2\tilde{V}_n^H(\mathbf{r})} \tag{5}$$

Note that the electric and magnetic polarizabilities α and β of the perturber have the units of a volume, implying that the induced electric and magnetic dipole moments of the perturber are given by $\mathbf{p}_{\mathrm{ind}} = \alpha\varepsilon_0 \tilde{\mathbf{E}}_n(\mathbf{r})$ and $\mathbf{m}_{\mathrm{ind}} = \beta\tilde{\mathbf{H}}n(\mathbf{r})/\mu_0$, where $n(\mathbf{r})$ is the refractive index. Equation 5 indicates that perturbation experiments may benchmark the magnetic interaction between light and matter as mediated by the complex magnetic modal volume and that the phase of the magnetic field of a QNM can be deduced with the knowledge of the polarizabilities.

This Letter addresses the topic of measurement and mapping of the magnetic modal volume in a photonic crystal cavity on slab. We provide experimental evidence that the magnetic perturbation theory should rely on non-Hermitian physics. In particular, we show that a coated metallic tip in a scanning near-field experiment acts as an anisotropic magnetic perturbation able to give access to the spatial distribution of the complex mode volume. This is an important result since $\tilde{V}_n^H(\mathbf{r})$ is deeply involved in light−matter interactions whenever the magnetic side of a photon plays a role, especially in the field of metamaterials and topological photonics.[10−12]

We analyze eq 5 in the case of a photonic crystal in a hexagonal array of holes on a dielectric slab. The cavity consists of four missing holes in a diamond geometry and was named as D2.[14,15] We numerically solve Maxwell's equations to find the QNMs, which are normalized using the QNM solver QNMEig[16] of the freely available package MAN (Modal Analysis of Nanoresonators). Therefore, we obtain the three components of the electric $\tilde{\mathbf{E}}_n(\mathbf{r})$ and three components of the magnetic $\tilde{\mathbf{H}}_n(\mathbf{r})$ fields for any QNM of the D2 cavity. Hereafter, we focus on the fundamental mode and further neglect to report the suffix n indicating the QNM index.

We also focus on hyperspectral scanning near-field optical microscopy (SNOM) experiments,[17] where the tip can be exploited both as a perturber at the nanoscale and as a probe of the complex eigenvalues.[7,14,15] As shown in refs 7 and 14, a chemically etched uncoated near-field fiber probe is a good approximation of a point-like nonabsorbing scatterer, described by an isotropic electric dipole polarizability α. In refs 15 and 18 it has been shown that a commercial Al-coated aperture near-field probe on a cavity in slab photonic crystal acts as a perturber, exhibiting both in-plane isotropic electric dipolar and anisotropic diamagnetic responses. Note also that in a photonic crystal on slab the component normal to the slab plane, $\tilde{E}_z^2(\mathbf{r})$, is small with respect to $\tilde{E}_x^2(\mathbf{r}) + \tilde{E}_y^2(\mathbf{r})$, and it will be neglected hereafter. The electric and magnetic polarizabilities of the Al-coated probe can, thus, be defined as $\overline{\alpha}_{ij} = \alpha\delta_{ij}$ ($\mathrm{Re}(\alpha) > 0$) and $\overline{\beta}_{ij} = -\beta\delta_{iz}\delta_{jz}$ ($\mathrm{Re}(\beta) > 0$). It was also reported that $\mathrm{Re}(\beta) > \mathrm{Re}(\alpha)$, which means that the Al-coated probe acts as an effective diamagnetic perturber by inducing a blue-shift of the mode resonant wavelength.[15,18] The electric and magnetic polarizabilities of the probe can be defined within this picture, as for typical SNOM experiments we expect to be able to address the two complex quantities either $\tilde{E}^2(\mathbf{r}) = \tilde{E}_x^2(\mathbf{r}) + \tilde{E}_y^2(\mathbf{r})$, or $\tilde{H}_z^2(\mathbf{r})$ via the following:

$$\frac{\Delta\tilde{\omega}_n}{\tilde{\omega}_n} = -\alpha\varepsilon_o(\tilde{E}_x^2(\mathbf{r}) + \tilde{E}_y^2(\mathbf{r})) - \beta\mu_o\tilde{H}_z^2(\mathbf{r}) \tag{6}$$

https://doi.org/10.1021/acsphotonics.0c01943
ACS Photonics 2021, 8, 1258−1263

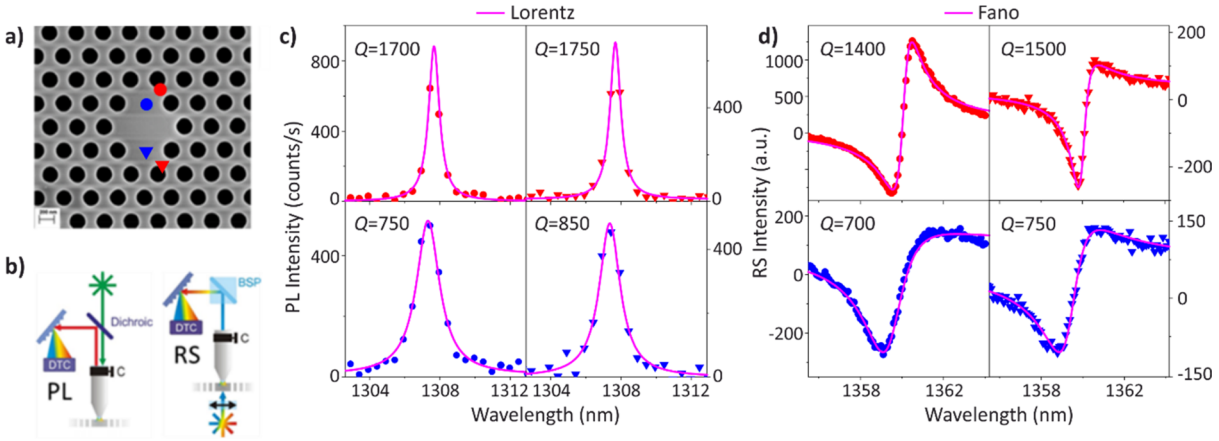

Figure 2. (a) Scanning electron microscope (SEM) image of a D2 cavity in which the red and blue symbols correspond to the symmetric positions where the SNOM spectra shown in (c) and (d) were taken. (b) Schemes of the PL and RS setups. (c) SNOM-PL spectra taken at the red (upper panels) and blue (lower panels) positions in (a) are shown as circles and triangles with the same color code; the magenta curves show the best Lorentzian fits. (d) SNOM-RS spectra recorder at the red (upper panels) and blue (lower panels) positions in (a); the magenta curves show the fitted Fano line shapes. In each spectrum, the Q evaluated from the fit is reported. Note that the unperturbed quality factor was around 2500 for both cavities.

In Figure 1a,b we report the results for the spatial distribution in an air plane at 20 nm above the slab of a D2 cavity of the real and imaginary parts of $\tilde{E}_x^2(\mathbf{r}) + \tilde{E}_y^2(\mathbf{r})$, and in Figure 1c,d we report the results for the spatial distribution of the real and imaginary parts of $\tilde{H}_z^2(\mathbf{r})$. In all maps the empty circles define the position of the air holes of the underlying photonic structures. With the knowledge of these field maps and the polarizabilities, the complex resonance frequency variations induced by the pointlike perturber given by a metallic SNOM tip at any position can be readily predicted by using eq 6.

Many general remarks can be done by inspecting these maps. The utmost relevant aspect in our discussion is that the imaginary parts of both fields show large regions with either positive or negative values of almost the same intensity. This means that, for a nonabsorbing scatterer, the real part of both polarizabilities α and β gives a variation of mode losses, which can be either positive or negative, thus inducing a change of Q. This evidence lies at the heart of the non-Hermitian perturbation theory and bears the modal volumes as complex quantities.[1,7] We notice that the real parts of both $\tilde{E}^2(\mathbf{r})$ and $\tilde{H}_z^2(\mathbf{r})$ are 3 orders of magnitude larger than their imaginary parts and that they do not change sign over space. In addition, they have the opposite sign, that is $\mathrm{Re}(\tilde{E}^2) > 0$ and $\mathrm{Re}(\tilde{H}_z^2) < 0$. All these features are common to any given spectrally isolated photonic mode with a relatively high Q and according to the original idea in ref 2 and following eq 4 and ref 5 in such a case, the Lorentzian line shape in the electric and magnetic LDOS is a very good approximation. Furthermore, $\mathrm{Re}(\tilde{H}_z^2) < 0$ is consistent with the definition of the complex magnetic volume possessing a negative sign (i.e., $\tilde{H}_z(r)$ is almost purely imaginary), and it gives the expected blue spectral shift of the diamagnetic polarizability when $\mathrm{Re}(\beta) > 0$.[15,18]

Another noteworthy feature is that the antinodes of $\mathrm{Re}(\tilde{E}^2)$ and $\mathrm{Re}(\tilde{H}_z^2)$ are found at the positions of the nodes of $\mathrm{Re}(\tilde{H}_z^2)$ and $\mathrm{Re}(\tilde{E}^2)$, respectively. This helps to disentangle the role of the dielectric and diamagnetic perturbation in near-field experiments. In refs 15 and 18, the experimental maps of the blue shift having a maximum at the antinode of the magnetic field map was indeed one key aspect to assess that a SNOM metallic tip mainly acts as an anisotropic diamagnetic perturber. It is worth stressing that in ref 15 the near-field map of the QNM spectral blue shift was compared to $|\tilde{H}_z(\mathbf{r})|^2$, as predicted by Hermitian perturbation theory; however, considering that $\tilde{H}_z$ is nearly a purely imaginary number, the approximation $-\mathrm{Re}(\tilde{H}_z^2(\mathbf{r})) \approx |\tilde{H}_z(\mathbf{r})|^2$ holds, hence, the Hermitian theory predictions for the blue shifts due to diamagnetic scatterers are quantitatively correct.

The novelty of the non-Hermitian perturbation theory in high Q photonic cavities with spectrally isolated QNMs are associated with the loss modulations, that is, the presence of spatial regions on top of the cavity with both positive and negative imaginary parts of the mode volume. In analyzing the experimental results, we aim to assess the nature of the induced loss modulation due to the scanning in the near-field of a metallic-coated SNOM tip. Therefore, as a first step, we select two points of the D2 photonic crystal cavity where the effect of a dielectric vs diamagnetic are expected to be opposite. These points are highlighted as yellow circles in Figure 1b,d.

Electron beam lithography followed by reactive ion etching was used to fabricate the perforated air-membrane.[14,15] InAs quantum dots were embedded in the GaAs membrane. Two different near field experiments were performed: photoluminescence (PL) and resonant scattering (RS) by using a Al-coated aperture near-field probe (LovaLite, Besancon, France),[15,19] which both collected the near-field light and acted as a local perturbation. The two setups are sketched in Figure 2b. In the PL experiments, we used illumination/collection configuration and the quantum dots were excited at 780 nm, and we detected the near-field photoluminescence under moderate state filling condition in order to have a large emission band around 1300 nm. The RS experiments were performed in transmission geometry where light coming from a supercontinuum laser (ranging from 1100−1500 nm) was focused on the sample surface on a spot of approximately 2 μm diameter size to ensure a homogeneous excitation on the entire cavity. The transmitted light was collected by the Al-coated probe that allowed us to filter out and reduce the contribution of nonresonant scattering channels, which is mandatory for good signal/noise RS experiments. In both PL and RS experiments, the tip remained fixed while the sample was raster scanned at a constant tip−sample distance of around 20

https://doi.org/10.1021/acsphotonics.0c01943
ACS Photonics 2021, 8, 1258−1263

nm, while detecting the optical signal collected by the same probe.

In Figure 2c (Figure 2d) we report PL (RS) spectra for the lower-energy D2 cavity mode obtained in the blue and red points highlighted in Figure 2a and corresponding to the yellow spots in Figure 1b,d and to their symmetric positions in the lower part of the cavity. It is worth stressing that here the LDOS line shape is almost Lorentzian for the selected QNM, as given by the PL spectrum; while the Fano profile of the RS spectrum arises from the interference forming the driving and the scattered fields.[19] By fitting the two recorded line shapes with Lorentzian (for PL) and Fano (for RS) profiles, we inferred the central resonance wavelength λ and the quality factor Q. Both these parameters change along the SNOM scanning due to the tip perturbation. However, in symmetric positions with respect to the center of the cavity, the Q value presents slight variations, as highlighted in Figure 2c,d, where the color and shape of the experimental data reproduce the code used to label the two investigated points on the cavity surface image in Figure 2a.

The PL and RS data refer to two independent experiments performed with two different SNOM tips as well as slightly different photonic cavities, as can be inferred from the almost 50 nm difference in the central wavelengths of the two resonances. Nevertheless, the QNM main features are very similar. The spectra taken in the blue points show a blue shift of the QNM resonance and a much smaller quality factor ($Q \sim 750$); note also that the unperturbed quality factor was around 2500 for both cavities. The emergence of a blue shift agrees with the previously discussed diamagnetic effect associated with the metal-coated tip perturbation.[15] The striking feature of these data is the large variation of Q between the two points with different colors that are only about 200 nm apart. The red points correspond, in both experiments, to a Q twice time larger; which compared with the predictions of Figure 1 confirms the dominance of the diamagnetic perturbation induced by a metal-coated tip.

The maps of the quality factor Q obtained from RS and PL data are given in Figure 3a and b, respectively. On top of the map we report the geometry of the D2 cavity with thin circles describing the air holes, as obtained from the morphological map measured during the SNOM scan. The distortion observed between the two main blue regions in the quality factor map of Figure 3a are ascribed to piezoelectric stage drift during the long scan (more than 1 h) highlighted by the positioning of the slab holes (white circles), which are found misaligned with respect to the designed honeycomb lattice. As already mentioned, the PL and RS experiments were performed on two different cavities and by different tips, therefore it is not surprising that the absolute Q values were slightly different. Nevertheless, the Q spatial modulations are very similar, denoting the robustness of the near-field perturbation method for getting insight on the spatial distribution of a confined photonic mode. Note that the black regions in all the maps refer to points were the signal was too small for performing a reliable line shape fit. The data for the spectral shift were found fully in agreement with previous PL results[15] and we avoid reporting them in order to better emphasize the novelty the Q map analysis.

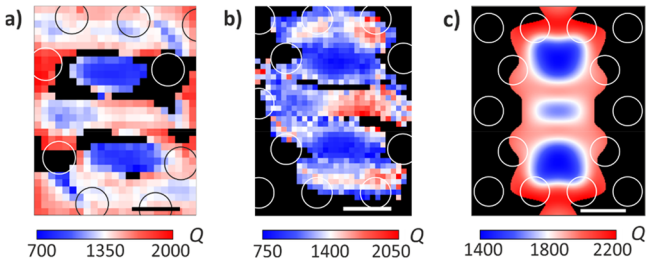

Figure 3. (a, b) Experimental map of the variation of Q for the RS and PL experiments, respectively. In both cases, the values of each Q were obtained by line shape fitting, as the examples reported in Figure 2c,d. Black pixels refer to points where the signal was too low for fitting the data. (c) Calculated map from eq 7 setting $\mathrm{Re}(\beta) \cong 20$, $\mathrm{Im}(\alpha) = 1.6 \times 10^{-2}\ \mu\mathrm{m}^{+3}$, $\Gamma_o = 2.5 \times 10^{-4}\omega_o$, and neglecting the terms in which $\mathrm{Re}(\alpha)$ and $\mathrm{Im}(\beta)$ appear. The scale bar is 300 nm.

Following the existing literature on the diamagnetic nature of the perturbation of an Al-coated tip,[18] that is, by assuming $\mathrm{Re}(\beta) > \mathrm{Re}(\alpha)$, we expect that the Q maps contain insights onto the imaginary part of the magnetic modal volume. This is indeed reflected in the two experimental Q modulations reported in Figure 3, where the main spatial features associated with the map of $\mathrm{Im}(\tilde{H}_z^2)$ can be recognized: two lobes exhibiting low Q positioned on the larger diagonal of the D2 cavity symmetrically to the center, which are surrounded externally by a region of higher Q.

A quantitative fit of these data is quite complex, since Al-coated SNOM tips are challenging objects to be modeled. In particular, the assumption that they induce an isotropic and homogeneous perturbation is questionable due to the heterogeneous nature of these tips, which exhibit a dielectric core and a metallic cover, without well-known thicknesses also due to tip damaging during a few scans. Moreover, the tips are not point-like dipoles in the plane since the dielectric aperture is about 100 nm and the extension of the metal coat thickness is almost 100 nm. The morphology in the vertical direction is even more complex and bulky, so we expect that the field gradients should play a relevant role. Since α and β are complex numbers, a quantitative analysis must take into account also the contribution of their imaginary parts, which give rise to Ohmic and scattering losses,[20] as demonstrated by the fact that the unperturbed Q values of the two cavities (measured by far-field experiments) is around $Q = 2500$. This means that, in general, the local damping $\Gamma(\mathbf{r})$ differs from the unperturbed value Γ_o by

$$\Gamma(\mathbf{r}) - \Gamma_o = \omega(\mathbf{r})[\mathrm{Im}(\alpha)\varepsilon_0\mathrm{Re}(\tilde{E}^2(\mathbf{r})) - \mathrm{Re}(\alpha)\varepsilon_0\mathrm{Im}(\tilde{E}^2(\mathbf{r})) - \mathrm{Im}(\beta)\mu_0\mathrm{Re}(\tilde{H}_z^2(\mathbf{r})) + \mathrm{Re}(\beta)\mu_0\mathrm{Im}(\tilde{H}_z^2(\mathbf{r}))] \quad (7)$$

It is important to note that the terms in which $\mathrm{Im}(\alpha)$ and $\mathrm{Im}(\beta)$ appear are both positive in all the points of the cavity, meaning that the Ohmic and scattering losses can only decrease the cavity Q.

In order to reproduce the experimental data by eq 7, the parameters α and β should be estimated, which requires a detailed model of the perturbing probe. This would imply a demanding knowledge of the geometry of the heterogeneous SNOM tip. To overcome this issue, we employed a phenomenological picture, including the minimum number of parameters, so neglecting $\mathrm{Re}(\alpha)$ with respect to $\mathrm{Re}(\beta)$ and $\mathrm{Im}(\alpha)$, according to the literature.[18] We chose to describe Ohmic and radiation losses by a single parameter, that is $\mathrm{Im}(\alpha)$. Then we evaluated the predictions of eq 7 by calculating the QNM map of the resulting quality factor

https://doi.org/10.1021/acsphotonics.0c01943
ACS Photonics 2021, 8, 1258−1263

$Q(r) \cong \frac{\omega_o}{2\Gamma(r)}$, where we neglected the small spectral shift using the unperturbed QNM frequency ω_o (i.e., $\omega(\mathbf{r}) = \omega_o$).

To reproduce the experimental maps, we chose the parameters of eq 7 to be $\mathrm{Re}(\beta) \cong 20\ \mathrm{Im}(\alpha) = 1.6 \times 10^{-2}\ \mu m^{+3}$ and $\Gamma_o = 2.5 \times 10^{-4}\omega_o$ (note, this is 20% larger than the experimental unperturbed value). In Figure 3c we reported the convolution of the calculated quality factor map with a two-dimensional Gaussian point-spread function with a full width at half-maximum of 100 nm in order to encompass the real size of our SNOM tip. In addition, to be consistent with the experimental data, we colored as black the pixels where the calculated intensity of the electric field was below a given threshold (10^{-3} of the maximum), so that near-field signal would be too weak to detect. The comparison shows that our calculations can reproduce the main features of the experimental maps. Despite the very rough modeling, we believe that our findings provide a qualitative method for imaging the imaginary part of the magnetic mode volume, a noteworthy result opening the way for a better understanding of the light−matter interaction mediated by the magnetic field.

In summary, we have shown that the QNM approach for describing photonics resonant states requires the use of complex mode volumes also for the magnetic side of the modes. Our results prove that even a commercial SNOM tip with Al-coating can induce a local perturbation on the mode quality factor that allows to retrieve the main spatial features of the QNM magnetic field. We expect that a carefully designed SNOM probe could give a more quantitative mapping of the magnetic modal volume, paving the way for a better understanding of the magnetic light−matter interaction, which we expect to be crucial especially in developing new metamaterials devices and for magnetic quantum emitters.

AUTHOR INFORMATION

Corresponding Author

Niccolò Caselli − *Department of Physical Chemistry, Universidad Complutense de Madrid, E28040 Madrid, Spain;* orcid.org/0000-0003-2609-3834; Email: ncaselli@ucm.es

Authors

Tong Wu − *LP2N, Institut d'Optique, CNRS, Université de Bordeaux, Talence 33400, France*

Guillermo Arregui − *Catalan Institute of Nanoscience and Nanotechnology (ICN2), CSIC and BIST, 08193 Bellaterra, Spain; Departamento de Física, Universitat Autònoma de Barcelona, 08193 Bellaterra, Spain*

Nicoletta Granchi − *LENS, University of Florence, Sesto Fiorentino 50019, Italy*

Francesca Intonti − *LENS, University of Florence, Sesto Fiorentino 50019, Italy*

Philippe Lalanne − *LP2N, Institut d'Optique, CNRS, Université de Bordeaux, Talence 33400, France;* orcid.org/0000-0003-1979-2290

Massimo Gurioli − *LENS, University of Florence, Sesto Fiorentino 50019, Italy;* orcid.org/0000-0002-6779-1041

Complete contact information is available at: https://pubs.acs.org/10.1021/acsphotonics.0c01943

Notes

The authors declare no competing financial interest.

ACKNOWLEDGMENTS

We are thankful to Silvia Vignolini for contributing to the PL experiments. We acknowledge the sample nanofabrication by Laurent Balet and Andrea Fiore, who are also thanked for many fruitful and interesting discussions. P.L. acknowledges NOMOS (ANR-18CE24-0026) and I-SQUAD (ANR-18CE47-0006) Projects for financial support. M.G. acknowledges funding from CdR Firenze (2018/24257).

REFERENCES

(1) Lalanne, P.; Yan, W.; Vynck, K.; Sauvan, C.; Hugonin, J. P. Light Interaction with Photonic and Plasmonic Resonances. *Laser Photonics Rev.* **2018**, *12* (5), 1−38.

(2) Sauvan, C.; Hugonin, J. P.; Maksymov, I. S.; Lalanne, P. Theory of the Spontaneous Optical Emission of Nanosize Photonic and Plasmon Resonators. *Phys. Rev. Lett.* **2013**, *110* (23), 1−5.

(3) Muljarov, E. A.; Langbein, W. Exact Mode Volume and Purcell Factor of Open Optical Systems. *Phys. Rev. B: Condens. Matter Mater. Phys.* **2016**, *94* (23), 1−19.

(4) Lassalle, E.; Bonod, N.; Durt, T.; Stout, B. Interplay between Spontaneous Decay Rates and Lamb Shifts in Open Photonic Systems. *Opt. Lett.* **2018**, *43* (9), 1950−1953.

(5) Pellegrino, D.; Balestri, D.; Granchi, N.; Ciardi, M.; Intonti, F.; Pagliano, F.; Silov, A. Y.; Otten, F. W.; Wu, T.; Vynck, K.; Lalanne, P.; Fiore, A.; Gurioli, M. Non-Lorentzian Local Density of States in Coupled Photonic Crystal Cavities Probed by Near- and Far-Field Emission. *Phys. Rev. Lett.* **2020**, *124* (12), 123902.

(6) Yang, J.; Giessen, H.; Lalanne, P. Simple Analytical Expression for the Peak-Frequency Shifts of Plasmonic Resonances for Sensing. *Nano Lett.* **2015**, *15* (5), 3439−3444.

(7) Cognée, K. G.; Yan, W.; La China, F.; Balestri, D.; Intonti, F.; Gurioli, M.; Koenderink, A. F.; Lalanne, P. Mapping Complex Mode Volumes with Cavity Perturbation Theory. *Optica* **2019**, *6* (3), 269−273.

(8) Yan, W.; Lalanne, P.; Qiu, M. Shape Deformation of Nanoresonator: A Quasinormal-Mode Perturbation Theory. *Phys. Rev. Lett.* **2020**, *125* (1), 13901.

(9) Doeleman, H. M.; Dieleman, C. D.; Mennes, C.; Ehrler, B.; Koenderink, A. F. Observation of Cooperative Purcell Enhancements in Antenna-Cavity Hybrids. *ACS Nano* **2020**, *14* (9), 12027−12036.

(10) Baranov, D. G.; Savelev, R. S.; Li, S. V.; Krasnok, A. E.; Alù, A. Modifying Magnetic Dipole Spontaneous Emission with Nanophotonic Structures. *Laser Photonics Rev.* **2017**, *11* (3), 1600268.

(11) Yen, T. J.; Padilla, W. J.; Fang, N.; Vier, D. C.; Smith, D. R.; Pendry, J. B.; Basov, D. N.; Zhang, X. Terahertz Magnetic Response from Artificial Materials. *Science (Washington, DC, U. S.)* **2004**, *303* (5663), 1494−1496.

(12) Lu, L.; Joannopoulos, J. D.; Soljačić, M. Topological Photonics. *Nat. Photonics* **2014**, *8* (11), 821−829.

(13) Lalanne, P. Mode Volume of Electromagnetic Resonators: Let Us Try Giving Credit Where It Is Due. *arXiv:2011.00218 [physics.optics]* **2020**, na.

(14) Intonti, F.; Vignolini, S.; Riboli, F.; Vinattieri, A.; Wiersma, D. S.; Colocci, M.; Balet, L.; Monat, C.; Zinoni, C.; Li, L. H.; Houdré, R.; Francardi, M.; Gerardino, A.; Fiore, A.; Gurioli, M. Spectral Tuning and Near-Field Imaging of Photonic Crystal Microcavities. *Phys. Rev. B: Condens. Matter Mater. Phys.* **2008**, *78* (4), 2−5.

(15) Vignolini, S.; Intonti, F.; Riboli, F.; Balet, L.; Li, L. H.; Francardi, M.; Gerardino, A.; Fiore, A.; Wiersma, D. S.; Gurioli, M. Magnetic Imaging in Photonic Crystal Microcavities. *Phys. Rev. Lett.* **2010**, *105* (12), 1−4.

(16) Yan, W.; Faggiani, R.; Lalanne, P. Rigorous Modal Analysis of Plasmonic Nanoresonators. *Phys. Rev. B: Condens. Matter Mater. Phys.* **2018**, *97* (20), 1−10.

(17) Novotny, L.; Hecht, B. *Principles of Nano-Optics: Cap 15*; Cambridge University Press: Cambridge, 2006.

(18) Burresi, M.; Kampfrath, T.; Van Oosten, D.; Prangsma, J. C.; Song, B. S.; Noda, S.; Kuipers, L. Magnetic Light-Matter Interactions

in a Photonic Crystal Nanocavity. *Phys. Rev. Lett.* **2010**, *105* (12), 1−4.
(19) Caselli, N.; Intonti, F.; La China, F.; Riboli, F.; Gerardino, A.; Bao, W.; Bargioni, A. W.; Li, L.; Linfield, E. H.; Pagliano, F.; Fiore, A.; Gurioli, M. Ultra-Subwavelength Phase-Sensitive Fano-Imaging of Localized Photonic Modes. *Light: Sci. Appl.* **2015**, *4*, e326.
(20) Sersic, I.; Tuambilangana, C.; Kampfrath, T.; Koenderink, A. F. Magnetoelectric Point Scattering Theory for Metamaterial Scatterers. *Phys. Rev. B: Condens. Matter Mater. Phys.* **2011**, *83*, 1−12.

https://doi.org/10.1021/acsphotonics.0c01943
ACS Photonics 2021, 8, 1258−1263